J Sci Comput (2018) 75:536–559
https://doi.org/10.1007/s10915-017-0546-0

Local Discontinuous Galerkin Methods for the Boussinesq Coupled BBM System

Joshua Buli[1] · **Yulong Xing**[2]

Received: 17 May 2017 / Revised: 19 August 2017 / Accepted: 24 August 2017 /
Published online: 2 September 2017

Abstract Nonlinear dispersive wave equations model a substantial number of physical systems that admit special solutions such as solitons and solitary waves. Due to the complex nature of the nonlinearity and dispersive effects, high order numerical methods are effective in capturing the physical system in computation. In this paper, we consider the Boussinesq coupled BBM system, and propose local discontinuous Galerkin (LDG) methods for solving the BBM system. For the proposed LDG methods, we provide two different choices of numerical fluxes, namely the upwind and alternating fluxes, as well as establish their stability analysis. The error estimate for the linearized BBM system is carried out for the LDG methods with the alternating flux. To present a time discretization that conserves the Hamiltonian numerically, the midpoint rule with a nontrivial nonlinear term in the discretization is proposed. Both Hamiltonian conserving and dissipating time discretizations are implemented, with multiple combinations of numerical flux and time discretization tested numerically. Numerical examples are provided to demonstrate the accuracy, long-time simulation, and Hamiltonian conservation properties of the proposed LDG methods for the coupled BBM system.

Keywords Local discontinuous Galerkin methods · Boussinesq system · Hamiltonian conservation · Coupled BBM system · Error estimate

Y. Xing: The work of this author was partially supported by the NSF Grants DMS-1621111, DMS-1753581 and ONR Grant N00014-16-1-2714.

✉ Yulong Xing
xing.205@osu.edu

Joshua Buli
jbuli001@ucr.edu

[1] Department of Mathematics, University of California Riverside, Riverside, CA 92521, USA

[2] Department of Mathematics, Ohio State University, Columbus, OH 43210, USA

1 Introduction

Nonlinear dispersive water wave models have numerous applications in a variety of engineering disciplines. One specific model is the Boussinesq approximation for water waves, which was developed by Joseph Boussinesq in 1871 [8] to take into account the vertical structure of the horizontal and vertical flow velocity. Derived from the Euler equations, this approximation results in nonlinear partial differential equations called Boussinesq-type equations, which incorporate frequency dispersion (as opposed to the nonlinear shallow water equations, where no frequency dispersion is present). In coastal engineering applications, Boussinesq-type equations are frequently used in computer models for the simulation of water waves in propagation of long-crested waves on the ocean, shallow seas, large lakes, coastlines, and harbors. These equations can also model water waves moving through a channel which have small amplitude and long wavelengths.

In practical applications, certain physical assumptions are made about the water waves, which lead to simplified mathematical models. A special case is the the abcd-Boussinesq systems which describe the propagation of small amplitude and long wavelength surface waves that are irrotational, incompressible, inviscid, and are influenced by gravity. In [5], the abcd-Boussinesq systems used to model such water waves are derived and given by

$$\begin{cases} \eta_t + u_x + (\eta u)_x + a u_{xxx} - b\eta_{xxt} = 0 \\ u_t + \eta_x + u u_x + c\eta_{xxx} - d u_{xxt} = 0, \end{cases} \tag{1.1}$$

where $\eta(x,t)$ represents proportional deviation of the free surface from its rest position, and $u(x,t)$ represents proportional horizontal velocity. The constant parameters a, b, c, and d are not taken arbitrarily, and are chosen via the following relationships:

$$a + b = \frac{1}{2}\left(\theta^2 - \frac{1}{3}\right), \quad c + d = \frac{1}{2}(1 - \theta^2) \geq 0, \tag{1.2}$$

with $\theta \in [0, 1]$, representing the scaled height (where $\theta = 0$ is the bottom of the channel and $\theta = 1$ is the free surface). In [5], seven different choices of the parameters are given, which lead to multiple types of Boussinesq systems including the classical Boussinesq sytem, Kaup system and Bona–Smith system etc. When there is no dispersive term, i.e., $a, b, c, d = 0$, the model (1.1) reduces to

$$\begin{cases} \eta_t + ((1+\eta)u)_x = 0 \\ u_t + (\eta + \frac{1}{2}u^2)_x = 0, \end{cases} \tag{1.3}$$

which is the shallow water equation if we replace $1 + \eta$ by water height h.

In this paper, we consider the coupled BBM system (taking $a = c = 0$ and $b = d = \frac{1}{6}$ or equivalently $\theta^2 = \frac{2}{3}$ in (1.2)), which is given by

$$\begin{cases} \eta_t + u_x + (\eta u)_x - \dfrac{1}{6}\eta_{xxt} = 0, \\ u_t + \eta_x + u u_x - \dfrac{1}{6}u_{xxt} = 0, \qquad (x,t) \in [a_0, a_1] \times [0, T], \end{cases} \tag{1.4}$$

subject to the initial conditions

$$u(x,0) = u_0(x), \qquad \eta(x,0) = \eta_0(x), \tag{1.5}$$

and periodic boundary conditions

$$u(a_0,t) = u(a_1,t), \qquad \eta(a_0,t) = \eta(a_1,t). \tag{1.6}$$

The systems in (1.4) are coupled nonlinear partial differential equations with weak dispersion effects resulting from the u_{xxt} and η_{xxt} terms. In the derivation of (1.1) (and therefore (1.4)), dissipative effects are not considered, and the system given in (1.4) admits the following Hamiltonian functionals

$$\int_{\mathbb{R}} \eta \, dx, \qquad \int_{\mathbb{R}} u \, dx, \qquad \int_{\mathbb{R}} (\eta u + \eta_x u_x) \, dx, \qquad \frac{1}{2} \int_{\mathbb{R}} \left[\eta^2 + (1+\eta) u^2 \right] \, dx. \tag{1.7}$$

The coupled BBM system is related to the single BBM equation, which was derived by Benjamin, Bona, and Mahoney in 1972 in [3]. The single BBM equation was developed as an alternative to the Korteweg–de Vries (KdV) equation. Recall the KdV equation given by

$$u_t + u_x + u u_x + u_{xxx} = 0, \tag{1.8}$$

and the single BBM equation can be written as

$$u_t + u_x + u u_x - u_{xxt} = 0, \tag{1.9}$$

where constants in front of the nonlinear and high-order terms have been suppressed. In [3], the assumptions involved in the derivation of the KdV equation are equally valid for the single BBM equation (1.9). The single BBM equation has some attractive features that the KdV equation lacks, one specific example is better dispersion properties resulting in stability in high wavenumber components (see [3] for details).

There have been a wide range of theoretical work and various numerical methods available for the coupled BBM system. Bona and Chen provided existence, uniqueness, and regularity results of the coupled BBM system in [4]. The derivation of the system (1.1), and well-posedness results were given for multiple cases of (1.1), including (1.4) in [5] and [6]. Previous work established that solutions to (1.4) may blow-up in finite time if $1 + \eta < 0$. Chen and Liu [10] extended the result relating to the Hamiltonian (1.10), that solutions to (1.4) would not blow-up in finite time if η was bounded from below. In [4], an unconditionally stable fourth-order accurate finite difference numerical scheme is developed for (1.4). In [1], the same numerical method from [4] was used to conduct an in depth analysis to compare the solutions to the single BBM equation and the coupled BBM system. Finite element methods have been designed for the two dimensional coupled BBM system in [17].

In recent years, high order accurate numerical schemes have attracted increasing attention in many computational fields. Among different high-order methods, the discontinuous Galerkin (DG) method is a class of finite element methods using completely discontinuous piecewise polynomial basis functions, which inherits the benefits of both finite element and finite volume methods (see [12,14,15,21], and [13] for a historic review). Advantages of DG methods are many, including the local conservativity, the ability for easy handling of complicated geometries and boundary conditions, the flexibility for *hp*-adaptivity, efficient parallel implementation, and easy coordination with finite volume techniques, making the methods very attractive in in a wide range of applications. The DG methods were later generalized to the local discontinuous Galerkin (LDG) methods by Cockburn and Shu in [16] to solve the convection–diffusion equations and partial differential equations with high order spatial derivatives, motivated by successful numerical experiments from Bassi and Rebay for the compressible Navier–Stokes equations [2]. Later, LDG methods have been designed for many nonlinear dispersive equations, and we refer to the review paper [26] for the latest development of the LDG method. Recently, there have been many studies in designing LDG methods which can conserve the energy or Hamiltonian of the model numerically. An energy conserving LDG method for the generalized KdV equation is proposed in [7]. Energy conserving LDG methods have also been designed for other type of equations, including

the second order wave equation [11,24], Camassa–Holm equation [20], Degasperis–Procesi equation [19], etc.

In the present paper, we discuss the derivation and development of LDG methods to solve the coupled BBM system (1.4), which conserve or dissipate the Hamiltonian functional

$$\mathcal{E}(\eta, u) = \frac{1}{2}\int_I \left[\eta^2 + (1+\eta)u^2\right] dx. \tag{1.10}$$

To that effect, we develop two different choices of numerical flux, where one choice (the alternating flux, to be defined in Sect. 2) conserves the Hamiltonian for long time simulations, and the second flux (upwind flux) adds numerical dissipation and has a Hamiltonian decreasing property. Optimal error estimate is derived for the linearized coupled BBM system. We have also experimented with two different types of time discretizations, the implicit second order midpoint rule which conserves the Hamiltonian, and the standard Runge–Kutta methods. Proof is provided to verify that the LDG method with the alternating flux, coupled with the midpoint rule temporal discretization, and a special nonlinear term discretization, conserves the discrete Hamiltonian exactly. Note that the Hamiltonian (1.10) is only guaranteed to be non-negative when $1+\eta \geq 0$. Under this condition, the stability of the LDG method follows from the Hamiltonian conservation (or dissipation). When such condition does not hold, we observe numerically that both Hamiltonian conserving and dissipative methods perform well. Numerical evidence is also provided to show that the Hamiltonian conserving methods have a smaller phase and shape error for the long time simulations.

The organization of the paper is as follows. In Sect. 2, we present an LDG method for the problem with two choices of numerical fluxes. We then prove the Hamiltonian conservation and dissipation properties for the alternating and upwind numerical fluxes, respectively. Section 3 is devoted to the error estimate of the proposed methods for the linearized equations. Temporal discretizations, along with their conservation property, are discussed in Sect. 4. Section 5 contains various numerical experiments that show the optimal convergence rates, long time simulations, solitary wave generations and collisions. Finally, concluding remarks are given in Sect. 6.

2 Local Discontinuous Galerkin Discretization

2.1 Notation

Given an interval $I = [a_0, a_1]$, we divide I into N subintervals and label each cell as $I_j = \left[x_{j-\frac{1}{2}}, x_{j+\frac{1}{2}}\right]$ for $j = 1, \ldots, N$. The center of each cell is given by $x_j = \frac{1}{2}\left(x_{j-\frac{1}{2}} + x_{j+\frac{1}{2}}\right)$, with mesh size $h_j = x_{j+\frac{1}{2}} - x_{j-\frac{1}{2}}$. We denote the maximal mesh size as $h = \max_{1\leq j\leq N} h_j$. Let V_h^k denote the piecewise polynomial space

$$V_h^k = \{v : v|_{I_j} \mid v \in P^k(I_j),\ j = 1, \ldots, N\}, \tag{2.1}$$

where $P^k(I_j)$ denotes the space of polynomials of degree k on the cell I_j. Functions in V_h^k are allowed to have discontinuities across the cell interface. The terms $v^-_{j+\frac{1}{2}}$ and $v^+_{j+\frac{1}{2}}$ represent the limit value of v at $x_{j+\frac{1}{2}}$ from the left cell I_j and the right cell I_{j+1}, respectively.

We let $u_h \in V_h^k$ denote the solution of the DG numerical method. The notations for the jump at the interface, and the average of the function are given by $[u_h] = u_h^+ - u_h^-$ and

$\{u_h\} = \frac{1}{2}\left(u_h^+ + u_h^-\right)$, respectively. The L^1 and L^2 norms over the interval I are given by $||\cdot||_1$ and $||\cdot||$, respectively. For shorthand notation, we define

$$(\phi, \psi)_{I_j} = \int_{I_j} \phi\psi \, dx, \qquad (\phi, \psi) = \sum_{j=1}^{N} \int_{I_j} \phi\psi \, dx. \tag{2.2}$$

2.2 The LDG Method

In this section, we describe the semi-discrete LDG method for (1.4) by discretizing the space with the LDG method, and leave the time continuous. Time discretizations will be discussed in Sect. 4. We start by rewriting (1.4) as a first order system:

$$\begin{aligned} &w_t + (\eta + q)_x = 0, && v_t + (u + p)_x = 0, \\ &w = u - \tfrac{1}{6} r_x, && v = \eta - \tfrac{1}{6} s_x, \\ &r = u_x, && s = \eta_x, \\ &q = \tfrac{1}{2} u^2, && p = \eta u. \end{aligned} \tag{2.3}$$

Here we introduce two new variables p, q to replace the nonlinear terms, for the purpose of designing Hamiltonian preserving methods later. Using the abbreviated notation and periodic boundary condition, we formulate the LDG method for the system (2.3) as the following: find $u_h, \eta_h, p_h, q_h, r_h, s_h, w_h, v_h \in V_h^k$, such that

$$((w_h)_t, \phi) - (\eta_h + q_h, \phi_x) - \sum_{j=1}^{N} (\tilde{\eta}_h + \widehat{q}_h)_{j+\frac{1}{2}} [\phi]_{j+\frac{1}{2}} = 0, \tag{2.4a}$$

$$(w_h, \psi) = (u_h, \psi) + \frac{1}{6}(r_h, \psi_x) + \frac{1}{6} \sum_{j=1}^{N} (\widehat{r_h})_{j+\frac{1}{2}} [\psi]_{j+\frac{1}{2}}, \tag{2.4b}$$

$$(r_h, \varphi) = -(u_h, \varphi_x) - \sum_{j=1}^{N} (\widehat{u}_h)_{j+\frac{1}{2}} [\varphi]_{j+\frac{1}{2}}, \tag{2.4c}$$

$$(q_h, \zeta) = \left(\frac{1}{2} u_h^2, \zeta\right), \tag{2.4d}$$

$$((v_h)_t, \rho) - (u_h + p_h, \rho_x) - \sum_{j=1}^{N} (\tilde{u}_h + \widehat{p}_h)_{j+\frac{1}{2}} [\rho]_{j+\frac{1}{2}} = 0, \tag{2.4e}$$

$$(v_h, \theta) = (\eta_h, \theta) + \frac{1}{6}(s_h, \theta_x) + \frac{1}{6} \sum_{j=1}^{N} (\widehat{s_h})_{j+\frac{1}{2}} [\theta]_{j+\frac{1}{2}}, \tag{2.4f}$$

$$(s_h, \lambda) = -(\eta_h, \lambda_x) - \sum_{j=1}^{N} (\widehat{\eta}_h)_{j+\frac{1}{2}} [\lambda]_{j+\frac{1}{2}}, \tag{2.4g}$$

$$(p_h, \vartheta) = (\eta_h u_h, \vartheta), \tag{2.4h}$$

for all test functions $\phi, \psi, \varphi, \zeta, \rho, \theta, \lambda, \vartheta \in V_h^k$. The hat and tilde terms $\widehat{u}_h, \tilde{u}_h, \widehat{\eta}_h$, etc., known as numerical fluxes, are the boundary terms at each cell interface obtained from the integration by parts. In the next two subsections, we will consider two different sets of numerical fluxes, namely the alternating and upwind fluxes, with different conservation properties.

2.3 Alternating Flux

The choice of alternating flux can be summarized in the following groups

$$\begin{cases} \widehat{u}_h = u_h^+, \\ \widehat{\eta}_h = \eta_h^-, \end{cases} \qquad \begin{cases} \widehat{u}_h = u_h^-, \\ \widehat{\eta}_h = \eta_h^+, \end{cases}$$

$$\begin{cases} \tilde{u}_h + \widehat{p}_h = u_h^+ + p_h^+, \\ \tilde{\eta}_h + \widehat{q}_h = \eta_h^- + q_h^-, \\ \widehat{r}_h = r_h^-, \\ \widehat{s}_h = s_h^+, \end{cases} \qquad \begin{cases} \tilde{u}_h + \widehat{p}_h = u_h^- + p_h^-, \\ \tilde{\eta}_h + \widehat{q}_h = \eta_h^+ + q_h^+, \\ \widehat{r}_h = r_h^+, \\ \widehat{s}_h = s_h^-, \end{cases}$$

where we can choose one bracketed group from row 1 for $\widehat{u}_h, \widehat{\eta}_h$, and one group from row 2 for the others. Note that the indices $j + \frac{1}{2}$ are dropped for convenience, as all fluxes above are computed at the same point at the cell boundary. It is emphasized that the choice of flux is not unique, as one can choose up to four different pairs of fluxes, as stated above. In this paper, we choose the ones on the left, namely,

$$\begin{aligned} &\widehat{u}_h = u_h^+, && \widehat{\eta}_h = \eta_h^-, \\ &\tilde{u}_h + \widehat{p}_h = u_h^+ + p_h^+, && \tilde{\eta}_h + \widehat{q}_h = \eta_h^- + q_h^-, \\ &\widehat{r}_h = r_h^-, && \widehat{s}_h = s_h^+, \end{aligned} \tag{2.5}$$

with the periodic boundary conditions on the boundary.

We now turn to establish the conservation of the Hamiltonian $\mathcal{E}(\eta, u)$ defined in (1.10).

Theorem 2.1 *The Hamiltonian*

$$\mathcal{E}_h(t) = \frac{1}{2} \int_I \left[\eta_h^2 + (1 + \eta_h) u_h^2 \right] dx \tag{2.6}$$

is conserved by the semi-discrete LDG method (2.4) *with the choice of alternating flux* (2.5).

Proof Choosing $\phi = u_h + p_h - (s_h)_t/6$ and $\rho = \eta_h + q_h - (r_h)_t/6$ in (2.4a) and (2.4e) respectively, we deduce

$$\begin{aligned} &\left((w_h)_t, u_h + p_h - \frac{1}{6}(s_h)_t \right) - \left(\eta_h + q_h, \left(u_h + p_h - \frac{1}{6}(s_h)_t \right)_x \right) \\ &\quad - \sum_{j=1}^{N} (\eta_h^- + q_h^-)_{j+\frac{1}{2}} \left[u_h + p_h - \frac{1}{6}(s_h)_t \right]_{j+\frac{1}{2}} = 0, \end{aligned} \tag{2.7a}$$

$$\begin{aligned} &\left((v_h)_t, \eta_h + q_h - \frac{1}{6}(r_h)_t \right) - \left(u_h + p_h, \left(\eta_h + q_h - \frac{1}{6}(r_h)_t \right)_x \right) \\ &\quad - \sum_{j=1}^{N} (u_h^+ + p_h^+)_{j+\frac{1}{2}} \left[\eta_h + q_h - \frac{1}{6}(r_h)_t \right]_{j+\frac{1}{2}} = 0. \end{aligned} \tag{2.7b}$$

Next, we take the time derivative of (2.4b) and (2.4f), and choose $\psi = u_h + p_h$ and $\theta = \eta_h + q_h$ to get

$$\begin{aligned} ((w_h)_t, u_h + p_h) = &((u_h)_t, u_h + p_h) + \left(\frac{1}{6}(r_h)_t, (u_h + p_h)_x \right) \\ &+ \frac{1}{6} \sum_{j=1}^{N} ((r_h)_t)_{j+\frac{1}{2}}^- [u_h + p_h]_{j+\frac{1}{2}}, \end{aligned} \tag{2.8a}$$

$$((v_h)_t, \eta_h + q_h) = ((\eta_h)_t, \eta_h + q_h) + \left(\frac{1}{6}(s_h)_t, (\eta_h + q_h)_x\right) + \frac{1}{6}\sum_{j=1}^{N}((s_h)_t)^+_{j+\frac{1}{2}}[\eta_h + q_h]_{j+\frac{1}{2}}. \tag{2.8b}$$

Add the equations in (2.7) and (2.8) respectively, then subtract the resulting equations to obtain

$$\begin{aligned} &-\frac{1}{6}((w_h)_t, (s_h)_t) - \frac{1}{6}((v_h)_t, (r_h)_t) + ((u_h)_t, u_h + p_h) + ((\eta_h)_t, \eta_h + q_h) \\ &= \frac{1}{6}\sum_{j=1}^{N}\left([(r_h)_t(u_h + p_h)] - [(r_h)_t](u_h^+ + p_h^+) - (r_h)_t^-[u_h + p_h]\right)_{j+\frac{1}{2}} \\ &\quad + \frac{1}{6}\sum_{j=1}^{N}\left([(\eta_h + q_h)(s_h)_t] - [\eta_h + q_h](s_h)_t^+ - (\eta_h^- + q_h^-)[(s_h)_t]\right)_{j+\frac{1}{2}} \\ &\quad - \sum_{j=1}^{N}\left([(\eta_h + q_h)(u_h + p_h)] - [\eta_h + q_h](u_h^+ + p_h^+) - (\eta_h^- + q_h^-)[u_h + p_h]\right)_{j+\frac{1}{2}} \\ &= 0, \end{aligned} \tag{2.9}$$

after we integrate the complete derivative out.

Next, take the time derivative of (2.4b) and (2.4f), and choose $\psi = (s_h)_t$ and $\theta = (r_h)_t$ to get

$$((w_h)_t, (s_h)_t) = ((u_h)_t, (s_h)_t) + \frac{1}{6}((r_h)_t, (s_h)_{tx}) + \frac{1}{6}\sum_{j=1}^{N}((r_h)_t)^-_{j+\frac{1}{2}}[(s_h)_t]_{j+\frac{1}{2}}, \tag{2.10a}$$

$$((v_h)_t, (r_h)_t) = ((\eta_h)_t, (r_h)_t) + \frac{1}{6}((s_h)_t, (r_h)_{tx}) + \frac{1}{6}\sum_{j=1}^{N}((s_h)_t)^+_{j+\frac{1}{2}}[(r_h)_t]_{j+\frac{1}{2}}. \tag{2.10b}$$

Similarly, taking $\varphi = (\eta_h)_t$ and $\lambda = (u_h)_t$ in the time derivative of (2.4c) and (2.4g) yields

$$((r_h)_t, (\eta_h)_t) = -((u_h)_t, (\eta_h)_{tx}) - \sum_{j=1}^{N}((u_h)_t)^+_{j+\frac{1}{2}}[(\eta_h)_t]_{j+\frac{1}{2}}, \tag{2.11a}$$

$$((s_h)_t, (u_h)_t) = -((\eta_h)_t, (u_h)_{tx}) - \sum_{j=1}^{N}((\eta_h)_t)^-_{j+\frac{1}{2}}[(u_h)_t]_{j+\frac{1}{2}}. \tag{2.11b}$$

Adding the equations in (2.10) and (2.11) together and using integration by parts, we obtain

$$\begin{aligned} ((w_h)_t, (s_h)_t) + ((v_h)_t, (r_h)_t) &= -\frac{1}{6}\sum_{j=1}^{N}\left([(r_h)_t(s_h)_t] - [(r_h)_t](s_h)_t^+ - (r_h)_t^-[(s_h)_t]\right)_{j+\frac{1}{2}} \\ &\quad + \sum_{j=1}^{N}\left([(\eta_h)_t(u_h)_t] - [(\eta_h)_t](u_h)_t^+ - (\eta_h)_t^-[(u_h)_t]\right)_{j+\frac{1}{2}} \\ &= 0. \end{aligned} \tag{2.12}$$

Combining the Eqs. (2.9) and (2.12), we have

$$((u_h)_t, u_h) + ((\eta_h)_t, \eta_h) + ((u_h)_t, p_h) + ((\eta_h)_t, q_h) = 0, \tag{2.13}$$

Therefore,

$$\begin{aligned}\frac{d}{dt}\frac{1}{2}\int_I \left(\eta_h^2 + (1+\eta_h)u_h^2\right)\, dx &= ((\eta_h)_t, \eta_h) + ((u_h)_t, u_h) + (u_h(u_h)_t, \eta_h) + ((\eta_h)_t, u_h^2/2) \\ &= ((u_h)_t, u_h) + ((\eta_h)_t, \eta_h) + ((u_h)_t, p_h) + ((\eta_h)_t, q_h) = 0 \end{aligned} \tag{2.14}$$

where the second equality comes from the Eqs. (2.4b) and (2.4f). □

Remark 2.1 Another choice of the numerical flux is the central flux, which is well-known for conserving the Hamiltonian exactly. It takes the form of

$$\begin{aligned} \widehat{u}_h &= \{u_h\}, & \widehat{\eta}_h &= \{\eta_h\}, \\ \tilde{u}_h + \widehat{p}_h &= \{u_h\} + \{p_h\}, & \tilde{\eta}_h + \widehat{q}_h &= \{\eta_h\} + \{q_h\}, \\ \widehat{r}_h &= \{r_h\}, & \widehat{s}_h &= \{s_h\}, \end{aligned} \tag{2.15}$$

and the same conclusion in Theorem 2.1 holds for the central flux. It is also known for the even-odd phenomenon of convergence rate, i.e., one can observe optimal convergence (of order $k+1$) if even order polynomial space (of degree k) is used, and suboptimal convergence (of order k) if odd order polynomial space is used. We have performed numerical simulations with central flux for the coupled BBM system and observed the same behavior. Therefore, we believe the alternating flux, which provides optimal convergence rate, is a better candidate for Hamiltonian-preserving methods.

2.4 Upwind Flux

The other set of numerical flux is the upwind flux, which is widely used for hyperbolic conservation laws to provide numerical dissipation. The choice of upwind flux for (1.4) can be summarized as

$$\begin{aligned} \widetilde{u}_h &= \{u_h\} - \frac{1}{2}[\eta_h], & \widetilde{\eta}_h &= \{\eta_h\} - \frac{1}{2}[u_h], \\ \widehat{q}_h &= \{q_h\} - \frac{1}{2}[p_h], & \widehat{p}_h &= \{p_h\} - \frac{1}{2}[q_h], \\ (\widehat{r}_h)_t &= \{(r_h)_t\} - \frac{1}{2}[(s_h)_t], & (\widehat{s}_h)_t &= \{(s_h)_t\} - \frac{1}{2}[(r_h)_t] \\ (\widehat{u}_h)_t &= \{(u_h)_t\} + \frac{1}{2}[(\eta_h)_t], & (\widehat{\eta}_h)_t &= \{(\eta_h)_t\} + \frac{1}{2}[(u_h)_t], \end{aligned} \tag{2.16}$$

With the above choice, we have the following theorem that shows the dissipation of the Hamiltonian $\mathcal{E}(\eta, u)$ over time.

Theorem 2.2 *For the semi-discrete LDG method* (2.4) *with the choice of upwind flux* (2.16)*, the Hamiltonian* $\mathcal{E}_h(t)$ *satisfies*

$$\frac{d}{dt}\mathcal{E}_h(t) = \frac{1}{2}\frac{d}{dt}\int_{\mathbb{R}} \left[\eta_h^2 + (1+\eta_h)u_h^2\right]\, dx \le -\frac{1}{12}\sum_{j=1}^{N}[(u_h)_t]^2 - \frac{1}{12}\sum_{j=1}^{N}[(\eta_h)_t]^2 \le 0, \tag{2.17}$$

for all time.

Proof We begin with the LDG method given by (2.4). In Eqs. (2.4a) and (2.4e), the test functions ϕ, ρ are taken to be $\phi = u_h + p_h - \frac{1}{6}(s_h)_t$ and $\rho = \eta_h + q_h - \frac{1}{6}(r_h)_t$. Summing up the resulting equations yields

$$\begin{aligned}
&\left((w_h)_t, u_h + p_h - \frac{1}{6}(s_h)_t\right) + \left((v_h)_t, \eta_h + q_h - \frac{1}{6}(r_h)_t\right) \\
&\quad = \left(\eta_h + q_h, \left(u_h + p_h - \frac{1}{6}(s_h)_t\right)_x\right) + \sum_{j=1}^{N} (\widetilde{\eta}_h + \widehat{q}_h)_{j+\frac{1}{2}} \left[u_h + p_h - \frac{1}{6}(s_h)_t\right]_{j+\frac{1}{2}} \\
&\qquad + \left(u_h + p_h, \left(\eta_h + q_h - \frac{1}{6}(r_h)_t\right)_x\right) + \sum_{j=1}^{N} (\widetilde{u}_h + \widehat{p}_h)_{j+\frac{1}{2}} \left[\eta_h + q_h - \frac{1}{6}(r_h)_t\right]_{j+\frac{1}{2}}.
\end{aligned} \tag{2.18}$$

Next, we take the sum of the time derivative of (2.4b) and (2.4f) with the test functions $\psi = u_h + p_h - \frac{1}{6}(s_h)_t$ and $\theta = \eta_h + q_h - \frac{1}{6}(r_h)_t$, which leads to

$$\begin{aligned}
&\left((w_h)_t, u_h + p_h - \frac{1}{6}(s_h)_t\right) + \left((v_h)_t, \eta_h + q_h - \frac{1}{6}(r_h)_t\right) \\
&\quad = \left((\eta_h)_t, \eta_h + q_h - \frac{1}{6}(r_h)_t\right) + \frac{1}{6}\left((s_h)_t, \left(\eta_h + q_h - \frac{1}{6}(r_h)_t\right)_x\right) \\
&\qquad + \frac{1}{6}\sum_{j=1}^{N} ((\widehat{s_h})_t)_{j+\frac{1}{2}} \left[\eta_h + q_h - \frac{1}{6}(r_h)_t\right]_{j+\frac{1}{2}} \\
&\qquad + \left((u_h)_t, u_h + p_h - \frac{1}{6}(s_h)_t\right) + \frac{1}{6}\left((r_h)_t, \left(u_h + p_h - \frac{1}{6}(s_h)_t\right)_x\right) \\
&\qquad + \frac{1}{6}\sum_{j=1}^{N} ((\widehat{r_h})_t)_{j+\frac{1}{2}} \left[u_h + p_h - \frac{1}{6}(s_h)_t\right]_{j+\frac{1}{2}}.
\end{aligned} \tag{2.19}$$

Subtracting (2.18) from (2.19), as well as regrouping these terms, we have

$$\begin{aligned}
&\left((\eta_h)_t, \eta_h + q_h - \frac{1}{6}(r_h)_t\right) + \left((u_h)_t, u_h + p_h - \frac{1}{6}(s_h)_t\right) \\
&\quad + \frac{1}{6}\left((s_h)_t, (\eta_h + q_h)_x\right) + \frac{1}{6}(\eta_h + q_h, (s_h)_{tx}) \\
&\quad + \frac{1}{6}\sum_{j=1}^{N} \left((\widehat{s_h})_t\,[\eta_h + q_h] + (\widetilde{\eta}_h + \widehat{q}_h)\,[(s_h)_t]\right)_{j+\frac{1}{2}} \\
&\quad + \frac{1}{6}\left((r_h)_t, (u_h + p_h)_x\right) + \frac{1}{6}(u_h + p_h, (r_h)_{tx}) \\
&\quad + \frac{1}{6}\sum_{j=1}^{N} \left((\widehat{r_h})_t\,[u_h + p_h] + (\widetilde{u}_h + \widehat{p}_h)\,[(r_h)_t]\right)_{j+\frac{1}{2}} \\
&\quad - \frac{1}{36}\left((s_h)_t, (r_h)_{tx}\right) - \frac{1}{36}(r_h, (s_h)_{tx}) - \frac{1}{36}\sum_{j=1}^{N} \left((\widehat{s_h})_t\,[(r_h)_t] + (\widehat{r_h})\,[(s_h)_t]\right)_{j+\frac{1}{2}}
\end{aligned}$$

$$
\begin{aligned}
&- \left(\eta_h + q_h, (u_h + p_h)_x\right) - (u_h + p_h, (\eta_h + q_h)_x) \\
&- \sum_{j=1}^{N} \left((\widetilde{\eta}_h + \widehat{q}_h)\,[u_h + p_h] + (\widetilde{u}_h + \widehat{p}_h)\,[\widetilde{\eta}_h + \widehat{q}_h]\right)_{j+\frac{1}{2}}. \qquad (2.20)
\end{aligned}
$$

Using the choice of upwind flux for $\widetilde{\eta}_h$, $\widetilde{u}_h$, $\widehat{q}_h$, $\widehat{p}_h$, $(\widehat{r}_h)_t$, and $(\widehat{s}_h)_t$ in (2.16), Eq. (2.20) reduces to

$$
\begin{aligned}
&\left((\eta_h)_t, \eta_h + q_h - \frac{1}{6}(r_h)_t\right) + \left((u_h)_t, u_h + p_h - \frac{1}{6}(s_h)_t\right) \\
&+ \sum_{j=1}^{N} \left(\frac{1}{6}[u_h + p_h][(s_h)_t] - \frac{1}{6}[\eta_h + q_h][(r_h)_t]\right. \\
&\left. + \frac{1}{72}[(r_h)_t]^2 + \frac{1}{72}[(s_h)_t]^2 + \frac{1}{2}[u_h + p_h]^2 + \frac{1}{2}[\eta_h + q_h]^2\right)_{j+\frac{1}{2}} = 0. \qquad (2.21)
\end{aligned}
$$

Now, we take the test functions $\varphi = \frac{1}{6}(\eta_h)_t$ and $\lambda = \frac{1}{6}(u_h)_t$ in the time derivative of (2.4c) and (2.4g), and sum up the resulting equations to obtain

$$
\begin{aligned}
&\frac{1}{6}((r_h)_t, (\eta_h)_t) + \frac{1}{6}((s_h)_t, (u_h)_t) \\
&\quad = -\frac{1}{6}((u_h)_t, (\eta_h)_{tx}) - \frac{1}{6}((\eta_h)_t, (u_h)_{tx}) - \frac{1}{6}\sum_{j=1}^{N} \left((\widehat{u}_h)_t[(\eta_h)_t] + (\widehat{\eta}_h)_t[(u_h)_t]\right)_{j+\frac{1}{2}} \\
&\quad = \frac{1}{12}\sum_{j=1}^{N} \left([(u_h)_t]^2 + [(\eta_h)_t]^2\right)_{j+\frac{1}{2}}, \qquad (2.22)
\end{aligned}
$$

with the choices of flux for $(\widehat{u}_h)_t$ and $(\widehat{\eta}_h)_t$ in (2.16). Summing up (2.21) and (2.22), we obtain

$$
\begin{aligned}
&((\eta_h)_t, \eta_h + q_h) + ((u_h)_t, u_h + p_h) \\
&+ \sum_{j=1}^{N} \left(\frac{1}{6}[u_h + p_h][(s_h)_t] - \frac{1}{6}[\eta_h + q_h][(r_h)_t] + \frac{1}{12}[(u_h)_t]^2 + \frac{1}{12}[(\eta_h)_t]^2\right. \\
&\left. + \frac{1}{72}[(r_h)_t]^2 + \frac{1}{72}[(s_h)_t]^2 + \frac{1}{2}[u_h + p_h]^2 + \frac{1}{2}[\eta_h + q_h]^2\right)_{j+\frac{1}{2}} = 0, \qquad (2.23)
\end{aligned}
$$

which leads to

$$
((\eta_h)_t, \eta_h + q_h) + ((u_h)_t, u_h + p_h) + \frac{1}{12}\sum_{j=1}^{N} [(u_h)_t]^2 + \frac{1}{12}\sum_{j=1}^{N} [(\eta_h)_t]^2 \le 0, \qquad (2.24)
$$

by Young's inequality. The same procedure in the alternating flux proof can be used to establish the following inequality

$$
\begin{aligned}
\frac{d}{dt}\frac{1}{2}\int_I \left(\eta_h^2 + (1 + \eta_h)u_h^2\right)\,dx &= ((u_h)_t, u_h) + ((\eta_h)_t, \eta_h) + ((u_h)_t, p_h) + ((\eta_h)_t, q_h) \\
&\le -\frac{1}{12}\sum_{j=1}^{N} [(u_h)_t]^2 - \frac{1}{12}\sum_{j=1}^{N} [(\eta_h)_t]^2 \le 0, \qquad (2.25)
\end{aligned}
$$

which completes the proof. □

3 Error Estimate for the Linearized System

In this section, we provide optimal error estimate for the linearized coupled BBM system when the alternating flux is used. The linearized coupled system takes the form of

$$\begin{cases} \eta_t + u_x - \eta_{xxt} = 0, \\ u_t + \eta_x - u_{xxt} = 0, \qquad (x,t) \in [a_0, a_1] \times [0,T], \end{cases} \tag{3.1}$$

where we have suppressed the constant coefficient $1/6$ for the ease of presentation. The LDG methods (2.4) then reduce to

$$\begin{aligned}
&((w_h)_t, \phi) - (\eta_h, \phi_x) - \sum_{j=1}^{N} (\tilde{\eta}_h)_{j+\frac{1}{2}} [\phi]_{j+\frac{1}{2}} = 0, \\
&(w_h, \psi) = (u_h, \psi) + (r_h, \psi_x) + \sum_{j=1}^{N} (\widehat{r_h})_{j+\frac{1}{2}} [\psi]_{j+\frac{1}{2}}, \\
&(r_h, \varphi) = -(u_h, \varphi_x) - \sum_{j=1}^{N} (\widehat{u_h})_{j+\frac{1}{2}} [\varphi]_{j+\frac{1}{2}}, \\
&((v_h)_t, \rho) - (u_h, \rho_x) - \sum_{j=1}^{N} (\tilde{u}_h)_{j+\frac{1}{2}} [\rho]_{j+\frac{1}{2}} = 0, \\
&(v_h, \theta) = (\eta_h, \theta) + (s_h, \theta_x) + \sum_{j=1}^{N} (\widehat{s_h})_{j+\frac{1}{2}} [\theta]_{j+\frac{1}{2}}, \\
&(s_h, \lambda) = -(\eta_h, \lambda_x) - \sum_{j=1}^{N} (\widehat{\eta_h})_{j+\frac{1}{2}} [\lambda]_{j+\frac{1}{2}}.
\end{aligned} \tag{3.2}$$

Let us introduce three projections to be used later. The first projection is the standard piecewise L^2 projection, which will be denoted as $\mathcal{P}$, with

$$\int_{I_j} (\mathcal{P}w(x) - w(x)) v(x)\, dx = 0 \qquad \text{for all } v \in P^k(I_j),\ \ j = 1, \cdots, N. \tag{3.3}$$

We also define $\mathcal{P}^+$ as a projection such that for a function w, $\mathcal{P}^+ w$ is the unique function in V_h^k satisfying

$$\int_{I_j} (\mathcal{P}^+ w(x) - w(x)) v(x)\, dx = 0 \qquad \text{for all } v \in P^{k-1}(I_j), \tag{3.4}$$

and

$$\mathcal{P}^+ w \left(x^+_{j-\frac{1}{2}} \right) = w \left(x_{j-\frac{1}{2}} \right) \qquad \text{for all } j. \tag{3.5}$$

Similarly, $\mathcal{P}^-$ is defined as

$$\int_{I_j} (\mathcal{P}^- w(x) - w(x)) v(x)\, dx = 0 \qquad \text{for all } v \in P^{k-1}(I_j), \tag{3.6}$$

and

$$\mathcal{P}^- w\left(x^-_{j+\frac{1}{2}}\right) = w\left(x_{j+\frac{1}{2}}\right) \qquad \text{for all } j. \tag{3.7}$$

All the projections mentioned previously satisfy the property (see [25] for details)

$$||\epsilon^w|| + h||\epsilon^w||_\infty + h^{\frac{1}{2}}||\epsilon^w||_{\Gamma_h} \le Ch^{k+1}, \tag{3.8}$$

where $\epsilon^w = \mathcal{P}w - w$ or $\epsilon^w = \mathcal{P}^\pm w - w$, Γ_h denotes the boundary points of all elements I_j, and C is a constant depending on w and independent of h.

We now provide the following theorem on the optimal error estimate for the linearized case when the alternating flux is used. One simplification, compared with the nonlinear problem, is that the linearized system yields an additional conserved quantity

$$\int_I (\eta^2 + u^2 + \eta_x^2 + u_x^2)\, dx, \tag{3.9}$$

which is helpful in the proof of the error estimate presented below. The approach presented here cannot be easily generalized to prove the optimal error estimate of the nonlinear system, as the quantity (3.9) is not conserved by the nonlinear system, therefore new ideas are needed for their error estimate.

Theorem 3.1 *Let u, η be the exact solutions to (3.1), and u_h, η_h be the numerical solution of the LDG scheme (3.2). Assume u, η have enough regularity, there holds the following error estimate:*

$$||u - u_h|| \le Ch^{k+1}, \qquad ||\eta - \eta_h|| \le Ch^{k+1}, \tag{3.10}$$

where the constant C depends on the final time T, k and the H^{k+1} norm of u, η up to time T.

Proof Let's define the shorthand operators $\mathcal{L}(f, g)$ and $\mathcal{R}(f, g)$ as

$$\mathcal{L}(f, g) = (f, g_x) + \sum_{j=0}^{N} f^+_{j+\frac{1}{2}}[g]_{j+\frac{1}{2}}, \qquad \mathcal{R}(f, g) = (f, g_x) + \sum_{j=0}^{N} f^-_{j+\frac{1}{2}}[g]_{j+\frac{1}{2}}. \tag{3.11}$$

Observe the following results of the above operators:

$$\mathcal{L}(f, g) + \mathcal{R}(g, f) = 0, \tag{3.12}$$

and

$$\mathcal{L}(\omega - \mathcal{P}^+\omega, g) = 0, \qquad \mathcal{R}(\omega - \mathcal{P}^-\omega, g) = 0, \qquad \text{for all } g \in V_h^k. \tag{3.13}$$

We will denote the following notations for the error estimate: $\xi^\omega = \mathbb{P}\omega - \omega_h$, $\epsilon^\omega = \mathbb{P}\omega - \omega$, and $e^\omega = \omega - \omega_h = \xi^\omega - \epsilon^\omega$, where ω stands for u, η, etc., and $\mathbb{P}$ is a projection that is to be chosen later in the proof. With these shorthand notations, we can write out the error equations based of the LDG method (3.2) for the linearized case

$$(e^w_t, \phi) = \mathcal{L}(e^\eta, \phi), \tag{3.14a}$$
$$(e^w, \psi) = (e^u, \psi) + \mathcal{L}(e^r, \psi), \tag{3.14b}$$
$$(e^r, \varphi) = -\mathcal{R}(e^u, \varphi), \tag{3.14c}$$
$$(e^v_t, \rho) = \mathcal{R}(e^u, \rho), \tag{3.14d}$$
$$(e^v, \theta) = (e^\eta, \theta) + \mathcal{R}(e^s, \theta), \tag{3.14e}$$
$$(e^s, \vartheta) = -\mathcal{L}(e^\eta, \vartheta). \tag{3.14f}$$

Subtract (3.14a) from the time derivative of (3.14b), and take the test functions $\phi = \psi = \xi^u$ to obtain

$$(e_t^u, \xi^u) + \mathcal{L}(e_t^r, \xi^u) - \mathcal{L}(e^\eta, \xi^u) = 0.$$

Applying the same procedure to (3.14d) and (3.14e) with the test functions $\phi = \psi = \xi^\eta$ yields

$$(e_t^\eta, \xi^\eta) + \mathcal{R}(e_t^s, \xi^\eta) - \mathcal{R}(e^u, \xi^\eta) = 0.$$

Taking the test functions $\varphi = \xi_t^r$, $\vartheta = \xi_t^s$ in (3.14c) and (3.14f) gives

$$(e^r, \xi_t^r) + \mathcal{R}(e^u, \xi_t^r) + (e^s, \xi_t^s) + \mathcal{L}(e^\eta, \xi_t^s) = 0.$$

Combining these equations and separating the error term e^ω as $\xi^\omega - \epsilon^\omega$, we have

$$\begin{aligned}
&(\xi_t^\eta, \xi^\eta) + (\xi_t^u, \xi^u) + (\xi^r, \xi_t^r) + (\xi^s, \xi_t^s) \\
&\quad = (\epsilon_t^\eta, \xi^\eta) + (\epsilon_t^u, \xi^u) + (\epsilon^r, \xi_t^r) + (\epsilon^s, \xi_t^s) \\
&\qquad + \mathcal{L}(\epsilon_t^r, \xi^u) + \mathcal{R}(\epsilon_t^s, \xi^\eta) - \mathcal{L}(\epsilon^\eta, \xi^u) - \mathcal{R}(\epsilon^u, \xi^\eta) + \mathcal{R}(\epsilon^u, \xi_t^r) + \mathcal{L}(\epsilon^\eta, \xi_t^s) \\
&\qquad - \mathcal{L}(\xi_t^r, \xi^u) - \mathcal{R}(\xi_t^s, \xi^\eta) + \mathcal{L}(\xi^\eta, \xi^u) + \mathcal{R}(\xi^u, \xi^\eta) - \mathcal{R}(\xi^u, \xi_t^r) - \mathcal{L}(\xi^\eta, \xi_t^s), \quad (3.15)
\end{aligned}$$

where the last line disappears following (3.12). If we take the projections of the variables as:

$$\mathbb{P}r = \mathcal{P}r \qquad \mathbb{P}s = \mathcal{P}s, \qquad \mathbb{P}u = \mathcal{P}^- u \qquad \mathbb{P}\eta = \mathcal{P}^+ \eta, \tag{3.16}$$

and utilize the relation (3.13), the error equation (3.15) becomes

$$\frac{1}{2}\frac{d}{dt}\left(||\xi^\eta||^2 + ||\xi^u||^2 + ||\xi^r||^2 + ||\xi^s||^2\right) = (\epsilon_t^\eta, \xi^\eta) + (\epsilon_t^u, \xi^u) + \mathcal{L}(\epsilon_t^r, \xi^u) + \mathcal{R}(\epsilon_t^s, \xi^\eta). \tag{3.17}$$

Applying the results in [23, Lemma 2.4] to Eqs. (3.14c) and (3.14f), we have the following estimates

$$||\xi_x^\eta||^2 + h^{-1}||[\xi^\eta]||_{\Gamma_h}^2 \le C_1||\xi^s||^2, \qquad ||\xi_x^u||^2 + h^{-1}||[\xi^u]||_{\Gamma_h}^2 \le C_1||\xi^r||^2, \tag{3.18}$$

which leads to

$$\begin{aligned}
\mathcal{L}(\epsilon_t^r, \xi^u) &= (\epsilon_t^r, \xi_x^u) + \sum_{j=0}^{N} \left(\epsilon_t^r\right)_{j+\frac{1}{2}}^+ [\xi^u]_{j+\frac{1}{2}} \\
&\le \frac{C_1}{2}||\epsilon_t^r||^2 + \frac{1}{2C_1}||\xi_x^u||^2 + \frac{C_1}{2}h||\left(\epsilon_t^r\right)^+||_{\Gamma_h}^2 + \frac{1}{2C_1}h^{-1}||[\xi^u]||_{\Gamma_h}^2 \\
&\le ||\xi^r||^2 + \frac{C_1}{2}||\epsilon_t^r||^2 + \frac{C_1}{2}h||\left(\epsilon_t^r\right)^+||_{\Gamma_h}^2 \\
&\le ||\xi^r||^2 + Ch^{2k+2}, \quad (3.19)
\end{aligned}$$

where the optimal error estimate of the projection error (3.8) is used in the last inequality. Similarly, we have

$$\mathcal{R}(\epsilon_t^s, \xi^\eta) \le ||\xi^s||^2 + Ch^{2k+2}. \tag{3.20}$$

Combining the inequalities (3.17), (3.19), and (3.20), we have

$$\frac{1}{2}\frac{d}{dt}\left(||\xi^\eta||^2 + ||\xi^u||^2 + ||\xi^r||^2 + ||\xi^s||^2\right) \le ||\xi^\eta||^2 + ||\xi^u||^2 + ||\xi^r||^2 + ||\xi^s||^2 + Ch^{2k+2}. \tag{3.21}$$

The optimal error estimate (3.10) follows from the Gronwall's inequality and the optimal error estimate of the projection error (3.8). □

4 Time Discretization

In this section, we present two different temporal discretizations that will be used to discretize the semi-discrete LDG methods (2.4) in time.

4.1 Strong Stability Preserving Runge–Kutta (SSPRK) Methods

In applications, higher order time discretizations are often required. A standard choice of high order time discretization is the well known class of SSPRK methods presented in [18]. Such methods pose nonlinear stability properties in the discretization of hyperbolic conservation laws. A variety of methods are presented in [18] including explicit, implicit, as well as multi-step SSPRK methods. In our numerical examples, we will use the five stages SSPRK4 scheme that is provided in [18,22], given by

$$
\begin{aligned}
u_h^{(1)} &= u_h^n + 0.391752226571890\Delta t\mathcal{L}(u_h^n),\\
u_h^{(2)} &= 0.444370493651235u_h^n + 0.555629506348765u_h^{(1)} + 0.368410593050371\Delta t\mathcal{L}(u_h^{(1)}),\\
u_h^{(3)} &= 0.620101851488403u_h^n + 0.379898148511597u_h^{(2)} + 0.251891774271694\Delta t\mathcal{L}(u_h^{(2)}),\\
u_h^{(4)} &= 0.178079954393132u_h^n + 0.821920045606868u_h^{(3)} + 0.544974750228521\Delta t\mathcal{L}(u_h^{(3)}),\\
u_h^{n+1} &= 0.517231671970585u_h^{(2)} + 0.096059710526147u_h^{(3)} + 0.063692468666290\Delta t\mathcal{L}(u_h^{(3)}),\\
&\quad + 0.386708617503269u_h^{(4)} + 0.226007483236906\Delta t\mathcal{L}(u_h^{(4)}),
\end{aligned}
$$

where $\mathcal{L}(\cdot)$ is the spatial discretization, which is taken to be the LDG method.

4.2 Midpoint Time Discretization

As the SSPRK method dissipates the Hamiltonian, we describe in this subsection an alternative midpoint rule time stepping scheme, which can conserve the discrete Hamiltonian in time.

Let $\{t_n\}_{n=0}^M$ be a partition of $[0, T]$ where $\Delta t^n = t^{n+1} - t^n$. Denote $\omega_h^n \in V_h$ (where $\omega = u, \eta, w, v$) as the numerical solution at time step n. We update in time via the following equation

$$\omega_h^{n+1} = 2\omega_h^{n,1} - \omega_h^n, \tag{4.1}$$

where $\omega_h^{n,1}$ are the solutions of the following equations

$$(\mathcal{D}w_h^n, \phi) - \left(\eta_h^{n,1} + q_h^{n,1}, \phi_x\right) - \sum_{j=1}^{N}(\tilde{\eta}_h^{n,1} + \widehat{q}_h^{n,1})_{j+\frac{1}{2}}[\phi]_{j+\frac{1}{2}} = 0, \tag{4.2a}$$

$$(w_h^{n,1}, \psi) - (u_h^{n,1}, \psi) - \frac{1}{6}(r_h^{n,1}, \psi_x) - \frac{1}{6}\sum_{j=1}^{N}(\widehat{r}_h^{n,1})_{j+\frac{1}{2}}[\psi]_{j+\frac{1}{2}} = 0, \tag{4.2b}$$

$$(r_h^{n,1}, \varphi) + (u_h^{n,1}, \varphi_x) + \sum_{j=1}^{N}(\widehat{u}_h^{n,1})_{j+\frac{1}{2}}[\varphi]_{j+\frac{1}{2}} = 0, \tag{4.2c}$$

$$(q_h^{n,1},\zeta)-\left(\frac{1}{4}\left((u_h^n)^2+(u_h^{n+1})^2\right),\zeta\right)=0, \tag{4.2d}$$

$$(\mathcal{D}v_h^n,\rho)-\left(u_h^{n,1}+p_h^{n,1},\rho_x\right)-\sum_{j=1}^{N}(\widetilde{u}_h^{n,1}+\widehat{p}_h^{n,1})_{j+\frac{1}{2}}[\rho]_{j+\frac{1}{2}}=0, \tag{4.2e}$$

$$(v_h^{n,1},\theta)-(\eta_h^{n,1},\theta)-\frac{1}{6}(s_h^{n,1},\theta_x)-\frac{1}{6}\sum_{j=1}^{N}(\widehat{s}_h^{n,1})_{j+\frac{1}{2}}[\theta]_{j+\frac{1}{2}}=0, \tag{4.2f}$$

$$(s_h^{n,1},\lambda)+(\eta_h^{n,1},\lambda_x)+\sum_{j=1}^{N}(\widehat{\eta}_h^{n,1})_{j+\frac{1}{2}}[\lambda]_{j+\frac{1}{2}}=0, \tag{4.2g}$$

$$(p_h^{n,1},\vartheta)-(\eta_h^{n,1}u_h^{n,1},\vartheta)=0, \tag{4.2h}$$

for all test functions $\phi,\psi,\varphi,\zeta,\rho,\theta,\lambda,\vartheta\in V_h^k$ and the notation $\mathcal{D}$ defined as

$$\mathcal{D}\omega_h^n=\frac{\omega_h^{n+1}-\omega_h^n}{\Delta t^n}=\frac{\omega_h^{n,1}-\omega_h^n}{\Delta t^n/2}. \tag{4.3}$$

Notice that special care is needed in the implementation of the midpoint rule on the non-linear terms in (4.2d), as the straightforward approach

$$(q_h^{n,1},\zeta)-\left(\frac{1}{2}(u_h^{n,1})^2,\zeta\right)=0,$$

will not yield a conservative time discretization.

In the following theorem, we will show that the discrete Hamiltonian is conserved exactly by the proposed LDG methods with alternating fluxes and midpoint rule time discretization.

Theorem 4.1 *The solution to the midpoint rule LDG method* (4.1) *and* (4.2)*, with the choice of alternating flux* (2.5)*, conserves the discrete Hamiltonian functional*

$$\mathcal{E}_h^n=\int\left[(\eta_h^n)^2+(1+(\eta_h^n))(u_h^n)^2\right]dx \tag{4.4}$$

for all n.

Proof Choosing $\phi=u_h^{n,1}+p_h^{n,1}-\frac{1}{6}\mathcal{D}s_h^{n,1}$ and $\rho=\eta_h^{n,1}+q_h^{n,1}-\frac{1}{6}\mathcal{D}r_h^{n,1}$ in (4.2a) and (4.2e) respectively, we get

$$\begin{aligned}&\left(\mathcal{D}w_h^n,u_h^{n,1}+p_h^{n,1}-\frac{1}{6}\mathcal{D}s_h^n\right)-\left(\left(\eta_h^{n,1}+q_h^{n,1}\right),\left(u_h^{n,1}+p_h^{n,1}-\frac{1}{6}\mathcal{D}s_h^n\right)_x\right)\\&-\sum_{j=0}^{N}(\widetilde{\eta}_h^{n,1}+\widehat{q}_h^{n,1})\left[u_h^{n,1}+p_h^{n,1}-\frac{1}{6}\mathcal{D}s_h^n\right]=0,\end{aligned} \tag{4.5a}$$

$$\begin{aligned}&\left(\mathcal{D}v_h^n,\eta_h^{n,1}+q_h^{n,1}-\frac{1}{6}\mathcal{D}r_h^n\right)-\left(\left(u_h^{n,1}+p_h^{n,1}\right),\left(\eta_h^{n,1}+q_h^{n,1}-\frac{1}{6}\mathcal{D}r_h^n\right)_x\right)\\&-\sum_{j=0}^{N}(\widetilde{u}_h^{n,1}+\widehat{p}_h^{n,1})\left[\eta_h^{n,1}+q_h^{n,1}-\frac{1}{6}\mathcal{D}r_h^n\right]=0.\end{aligned} \tag{4.5b}$$

Then, following the exact same steps as in the proof of Theorem 2.1, we can derive

$$(\mathcal{D}u_h^n,u_h^{n,1})+(\mathcal{D}u_h^n,p_h^{n,1})+(\mathcal{D}\eta_h^n,\eta_h^{n,1})+(\mathcal{D}\eta_h^n,q_h^{n,1})=0, \tag{4.6}$$

which is an analogue of Eq. (2.13). From the definition of $\mathcal{D}$, we obtain

$$\mathcal{D}u_h^n\, u_h^{n,1} = \frac{u_h^{n+1}-u_h^n}{\Delta t^n}\frac{u_h^{n+1}+u_h^n}{2} = \frac{(u_h^{n+1})^2-(u_h^n)^2}{2\Delta t^n}, \qquad \mathcal{D}\eta_h^n\, \eta_h^{n,1} = \frac{(\eta_h^{n+1})^2-(\eta_h^n)^2}{2\Delta t^n},$$

and also

$$\begin{aligned}
&(\mathcal{D}u_h^n,\, p_h^{n,1}) + (\mathcal{D}\eta_h^n,\, q_h^{n,1}) = (\eta_h^{n,1}u_h^{n,1},\, \mathcal{D}u_h^n) + \left(\frac{1}{4}\left((u_h^n)^2+(u_h^{n+1})^2\right),\, \mathcal{D}\eta_h^n\right)\\
&= \left(\frac{\eta_h^{n+1}+\eta_h^n}{2}\frac{u_h^{n+1}+u_h^n}{2},\, \frac{u_h^{n+1}-u_h^n}{\Delta t^n}\right) + \left(\frac{1}{4}\left((u_h^n)^2+(u_h^{n+1})^2\right),\, \frac{\eta_h^{n+1}-\eta_h^n}{\Delta t^n}\right)\\
&= \frac{\eta_h^{n+1}(u_h^{n+1})^2-\eta_h^n(u_h^n)^2}{2\Delta t^n},
\end{aligned}$$

where the approximation of nonlinear terms in (4.2d) and (4.2h) is used in the first equality. Combining these together, we conclude the result that $\mathcal{E}_h^{n+1} = \mathcal{E}_h^n$. □

5 Numerical Experiments

In this section numerical results are presented for the proposed LDG method (2.4) for the coupled BBM system (1.4). We will numerically test or validate the issues including the convergence rate, Hamiltonian conservation or dissipation, and their long time behavior. The third order finite element LDG methods (polynomials of degree $k = 2$), coupled with the two different types of time discretizations given in the previous section, are implemented in the numerical experiments.

To check accuracy and convergence rates, exact solutions are needed. One set of exact solutions is the traveling wave solutions presented in [9]:

$$\begin{aligned}
u(x,t) &= 3k\ \mathrm{sech}^2\left(\frac{3}{\sqrt{10}}(x-kt-x_0)\right),\\
\eta(x,t) &= \frac{15}{4}\left(-2+\cosh\left(3\sqrt{\frac{2}{5}}(x-kt-x_0)\right)\right)\mathrm{sech}^4\left(\frac{3}{\sqrt{10}}(x-kt-x_0)\right),
\end{aligned} \tag{5.1}$$

where $k = \pm\frac{5}{2}$, and x_0 denote the center of the wave at $t = 0$. The initial condition can be obtained from (5.1), i.e., $u_0(x) = u(x,0)$ and $\eta_0(x) = \eta(x,0)$.

5.1 Accuracy Test

The accuracy of our proposed LDG methods will be tested for a combination of numerical fluxes and time discretizations. The exact traveling wave solutions (5.1) on the domain $[0, L]$ with $L = 40$ are used. We first test the LDG method with the alternating fluxes, combined with both fourth order RK method and the second order midpoint rule. The time step size of midpoint rule is taken as $\Delta t = c\Delta x^2$ to be consistent with the fourth order RK method. Their numerical errors and the orders of convergence of the variables η_h and u_h are listed in Tables 1, 2. The exact parameters for each test case, including the time step size, spatial step size, are given in the caption of each table. From the tables, we can clearly see that the proposed LDG methods with alternating flux achieve the optimal convergence rates of 3 if the P^2 elements are used. To test the accuracy of the proposed LDG method with the upwind flux, with the fourth order RK method, we implement it on the exact traveling wave

Table 1 Convergence rate test for the alternating flux in space and SSPRK4 in time for the traveling wave solutions (5.1)

Parameters
$k = 2$, $L = 40$, $\Delta x = \frac{1}{2^j}$ for $j = 0, \ldots, 4$, $\Delta t = .1\Delta x$, $T = 1$

Nx	j	$\|e^{\eta}\|_{L^1}$	Order	$\|e^{u}\|_{L^1}$	Order
40	0	1.6003e−00		9.3584e−01	
80	1	1.5717e−01	3.34	6.9160e−02	3.75
160	2	1.5362e−02	3.35	5.0564e−03	3.77
320	3	1.7227e−03	3.15	5.2204e−04	3.27
640	4	2.0514e−04	3.06	6.4118e−05	3.02

Table 2 Convergence rate test for the alternating flux in space and 2nd order midpoint rule in time for the traveling wave solutions (5.1)
Parameters
$k = 2$, $L = 40$, $\Delta x = \frac{1}{2^j}$ for $j = 0, \ldots, 4$, $\Delta t = .1\Delta x^2$, $T = 1$, tolerance $= 10^{-10}$

Nx	j	$\|e^{\eta}\|_{L^1}$	Order	$\|e^{u}\|_{L^1}$	Order
40	0	2.1994e−00		1.5848e−00	
80	1	1.7709e−01	3.63	1.1434e−01	3.79
160	2	1.5581e−02	3.50	7.0977e−03	4.00
320	3	1.6858e−03	3.20	6.0759e−04	3.54
640	4	1.9711e−04	3.09	6.7434e−05	3.17

Table 3 Convergence rate test for the upwind flux in space and SSPRK4 in time for the traveling wave solutions (5.1)

Parameters
$k = 2$, $L = 40$, $\Delta x = \frac{1}{2^j}$ for $j = 0, \ldots, 4$, $\Delta t = .1\Delta x$, $T = 1$

Nx	j	$\|e^{\eta}\|_{L^1}$	Order	$\|e^{u}\|_{L^1}$	Order
40	0	1.6629e−00		1.0943e−00	
80	1	1.1121e−01	3.90	1.1281e−01	3.28
160	2	8.0167e−03	3.79	1.2562e−02	3.17
320	3	7.3197e−04	3.45	1.5346e−03	3.03
640	4	7.8245e−05	3.23	1.9317e−04	2.99

solutions (5.1). We document the L^1 error of the LDG solutions and list the results in Table 3, respectively. Again, we can easily observe the desired third order rate of convergence.

5.2 Comparisons of Different Numerical Flux and Time Discretization

In this section, we investigate the long time behavior of the proposed LDG methods to provide comparison of different choices of numerical flux and time discretizations.

First, we will compare the difference in the (Hamiltonian dissipating) RK and (Hamiltonian conserving) midpoint rule temporal discretizations, while keeping the spatial discretization as the LDG method with alternating flux. In this simulation, we take the exact traveling wave solutions (5.1) with $t = 0$ as the initial condition. The parameters in the initial condition are taken as follows: $x_0 = 20$ and $L = 40$, so that the peak of $u(x, 0)$ and the trough of $\eta(x, 0)$ are located at the center of the domain. We take the boundary conditions to be periodic, so that the wave will return to the initial profile after one period (with $T = 16$). Discretizaitons of space and time are taken to be $\Delta x = 0.25$ and $\Delta t = 0.1\Delta x^2$.

The alternating flux with the SSPRK4 and midpoint rule time discretizations achieve the correct order of accuracy for short time simulations, as indicated in the tables in the previous subsection. In this test, we run the simulation for a long time, up to $T = 180$ which corresponds to about eleven periods of the domain. The numerical solutions with three time discretizaitons (SSPRK2, SSPRK4, midpoint rule), compared with the exact solutions, at times $T = 60$, 130, and 180 are shown in Fig. 1. At time $T = 60$, no visual difference among different solutions can be observed. When time increases to 130, we can see that the

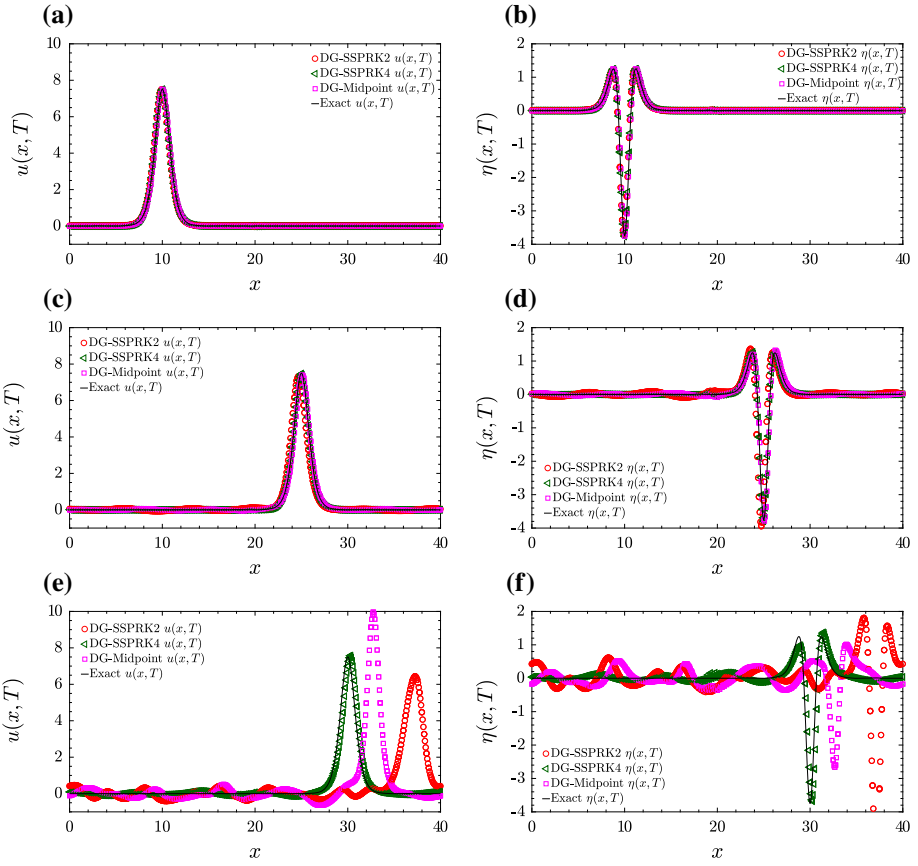

Fig. 1 Wave profiles for time discretization comparison. **a** Comparison between the SSPRK2, SSPRK4, and midpoint rule time discretizations for $u(x, T = 60)$, using the exact solitary wave initial condition; **b** comparison for $\eta(x, T = 60)$; **c** comparison for $u(x, T = 130)$; **d** comparison for $\eta(x, T = 130)$; **e** comparison for $u(x, T = 180)$; **f** comparison for $\eta(x, T = 180)$

SSPRK4 method performs slightly better. At $T = 180$, the fourth order SSPRK4 method clearly outperforms the other two, and midpoint rule is better than the second order SSPRK2 method with the same time step size. In Fig. 2, we plot the time history of the L^1 error between the exact solution and the numerical solutions up to $T = 180$. The error of SSPRK2 remains the largest one, and the error of midpoint rule and SSPRK4 are similar until $T = 120$, after which, the midpoint rule error increases much faster than the SSPRK4 scheme. It should be reiterated that the alternating flux-SSPRK4 method is order 3 in space and order 4 in time, whereas the alternating flux-midpoint rule method is order 3 in space and order 2 in time. As time progresses, the time error is compounded and begins to dominate.

The lower plot in Fig. 1 demonstrates the time history of the Hamiltonian that was proven for the midpoint rule with the alternating flux. It was shown in Sect. 4 that the discrete Hamiltonian (4.4) is conserved exactly in time for the midpoint rule. The fluctuations in the conserved quantity for the midpoint rule are extremely small, on the order of 10^{-10}, while the decay in the SSPRK4 method is on the order of 10^{-5}. The deviation of the conserved quantity for the SSPRK2 is much larger, as seen in the plot. This test shows that, with the

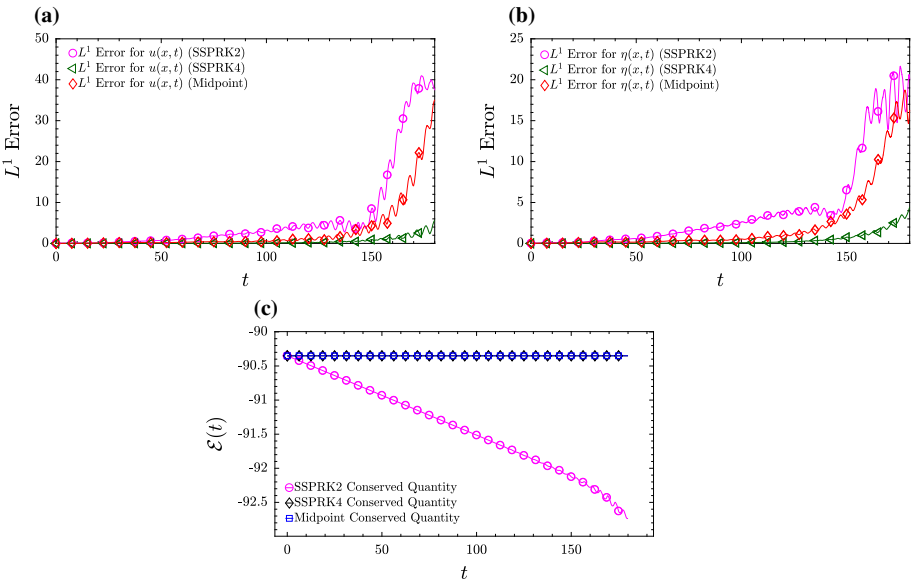

Fig. 2 Error and conserved quantity plots for time discretization comparison. **a** L^1 errors over time for $u(x,t)$, for the LDG numerical approximation using each time scheme; **b** L^1 errors for $\eta(x,t)$; **c** the computed value of the Hamiltonian (4.4) plotted over time for each choice of time discretization

same spatial discretization, the Hamiltonian conserving midpoint rule performs better than the Hamiltonian dissipative SSPRK2 method, but the higher order SSPRK4 (which dissipates Hamiltonian slightly) provides the best numerical solution. In the numerical experiments below, we will fix the SSPRK4 as the temporal discretization.

We now turn to looking at the difference between the choices of numerical flux on the same traveling wave solution. We will keep the choice of time discretization fixed as the SSPRK4 method, and compare the results of the alternating and upwind fluxes. We use the same initial condition as in the comparison of time discretizations in the previous paragraphs. The parameters of the simulation are taken to be: $x_0 = 20$, $L = 40$, $\Delta x = 0.25$, and $\Delta t = 0.1\Delta x$. Both choices of flux are comparable in terms of L^1 error up to about $T = 20$. After this point, the discrepancy between the errors in the alternating flux and upwind flux become evident. In Fig. 3, the comparison of both numerical solutions and the exact solution are provided at various times. We can observe that the upwind flux approximation is lagging behind the exact traveling wave solution, while the alternating flux approximation is essentially the same as the exact solution. The time history of the L^1 error and conserved Hamiltonian is shown in Fig. 4, which shows a larger error produced by the upwind flux. In terms of the Hamiltonian, the approximations verify that the Hamiltonian is constant for the alternating flux approximation, and the Hamiltonian is decreasing over time for the upwind flux.

5.3 Solitary Wave Generation

In this subsection, we perform the test to generate solitary waves (with $1 + \eta \geq 0$), as was done in [9] for their finite difference scheme. Generating such clean solitary waves is difficult in the physical laboratory setting, but can be easily done numerically using the procedure given in [9], and outlined as follows. This solitary wave solution will also be used in the next subsection to test the head-on collisions of solitary waves.

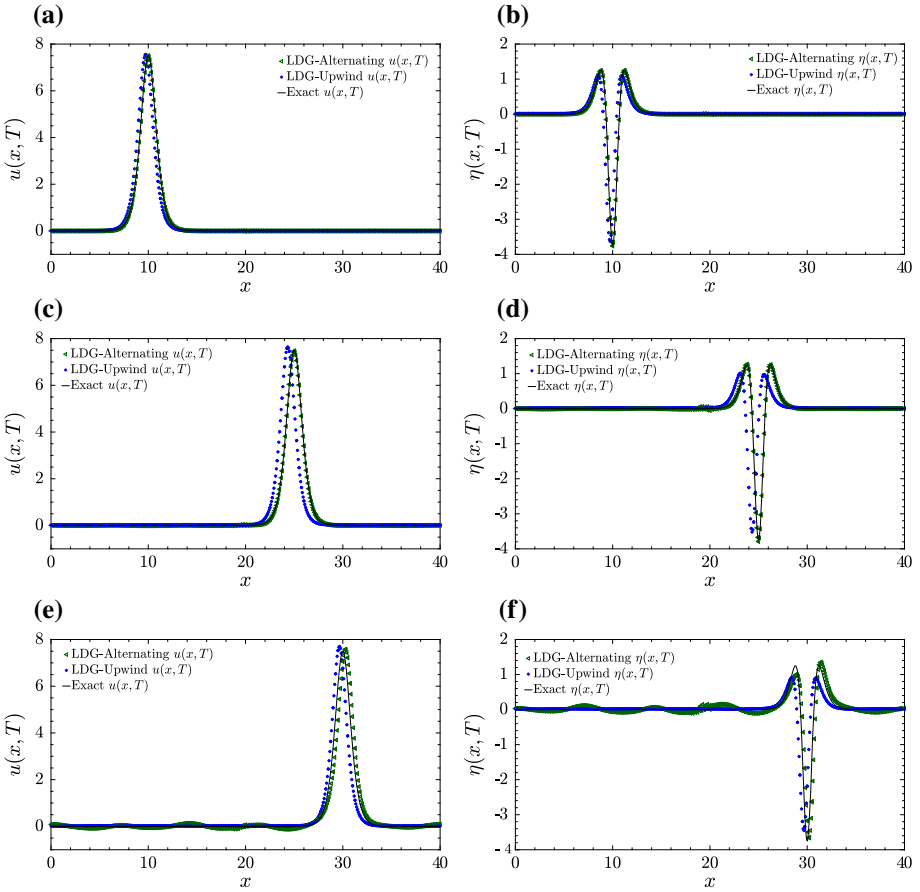

Fig. 3 Wave profiles for alternating and upwind comparison. **a** Comparison between the alternating and upwind choices for $u(x, T = 60)$, using the exact solitary wave initial condition. **b** Comparison for $\eta(x, T = 60)$. **c** Comparison for $u(x, T = 130)$. **d** Comparison for $\eta(x, T = 130)$. **e** Comparison for $u(x, T = 180)$. **f** Comparison for $\eta(x, T = 180)$

The coupled BBM system (1.4) is provided with the following initial condition

$$\eta(x,0) = N_0 \ \mathrm{sech}^2\left(\frac{1}{2}\sqrt{\frac{3N_0}{\kappa}}(x - x_0)\right),$$
$$u(x,0) = \eta(x,0) - \frac{1}{4}\eta^2(x,0), \tag{5.2}$$

with the parameters taken as $x_0 = 12$, $\kappa = 1 + \frac{1}{2}N_0$, and $N_0 = 0.7$, so that the peaks of $u(x, 0)$ and $\eta(x, 0)$ are located close to the left boundary of the domain. We take the boundary conditions to be periodic, and the length of the domain to be $L = 120$. Other numerical parameters are taken as $\Delta x = 0.25$ and $\Delta t = 0.1\Delta x$.

The initial wave (5.2) is provided to the LDG method and run up to a particular time, denoted as T. Here we chose $T = 48$ for the first run, but this value is arbitrary. The wave is evolved until the oscillations that are produced near the peaks are of small amplitude. Since

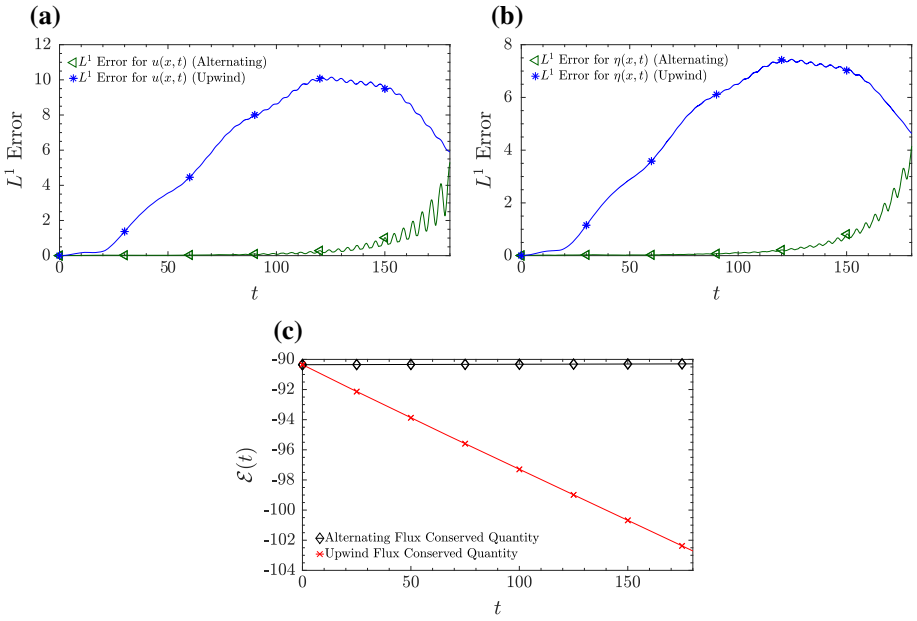

Fig. 4 Error and conserved quantity plots for alternating and upwind comparison. **a** L^1 errors over time for $u(x,t)$, for the LDG numerical approximation using each numerical flux. **b** L^1 errors for $\eta(x,t)$. **c** The computed value of the Hamiltonian (4.4) plotted over time for each choice of time discretization

we are using periodic boundary conditions, the only requirement of T is that the simulation must be stopped before any dispersive tails coming from the right interfere with the main wave (alternatively, one can use Dirichlet boundary conditions). The longer domain ($L = 120$ as opposed to $L = 40$ in previous tests) allows for the wave to travel farther before the dispersive tails become an issue. Once at time $T = 48$, the solution on the entire domain is clipped near the peak, such that the main peaks are spliced out of the domain. We inspect the amplitude of $\eta(x, T)$ and choose an subinterval of length 20 which contains the main peak, and save the LDG approximation from the subinterval.[1] The saved subinterval is then shifted and reloaded as the initial condition, so that the peak is again located at $x_0 = 20$, and then set $u(x, 0) \equiv 0$ and $\eta(x, 0) \equiv 0$ for the remaining portion of the domain. The clock is reset to $t = 0$, and the LDG code is run again up to a time where the main peak can be clipped again, using the described procedure. This setup allows the wave that was evolved in a previous run to be used as the initial condition in the subsequent run, but without the dispersive tails. The simulation is ran for a second time, up until $T = 48$. This procedure can be repeated as many times as possible, to reduce the magnitude of the dispersive tails. Alternatively, one can use a very long domain, and run the simulation one time for a larger value of T. We have also used this method with $L = 400$, yielding similar results.

Figure 5 shows the evolution and filtering of the solitary wave by the LDG method with alternating flux and SSPRK4 time discretization. In Fig. 5a, the initial condition (5.2) for $\eta(x, t)$ is plotted. Figure 5b shows the evolution of $\eta(x, t)$, which is the wave profile (Recall $u(x, t)$, which is not shown, is the horizontal velocity of the wave) at time $T = 48$. The dispersive tails emanating behind the main peak are evident. We can now excise the main

[1] The length of this subinterval is arbitrary. We wish to capture the peak in the interval, and have the "tails" near the peak to be close to zero.

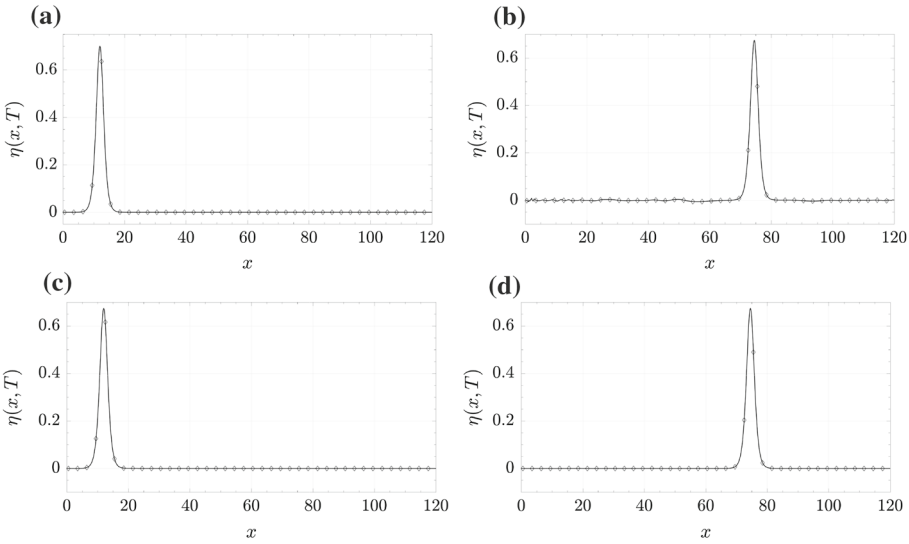

Fig. 5 Clean solitary wave generation for $\eta(x,t)$. **a** Initial condition for the solitary wave generation. **b** Equation (1.4) evolves up to $T = 48$ for the first run. **c** The peak of the solitary wave is excised from (**b**) and inserted so that the peak is located at $x_0 = 12$, as in figure (**a**). **d** The initial profile from (**c**) evolved to $T = 48$, and no visible oscillations are present

peak from this wave profile, which can be used for another filtering step. The filtering step reduces the magnitude of the oscillation, as can be seen in Fig. 5d, where on visual inspection, the oscillations cannot be seen. The magnitude of the oscillations in this figure is on the order of 10^{-5} after one filtering step.

5.4 Solitary Wave Collisions

In this example, we present a simulation for the head-on collision of two solitary waves of the same height, using the clean solitary waves generated in the previous subsection. We use the functions given in (5.2) to generate a right moving solitary wave, and we use

$$\widetilde{\eta}(x,0) = \eta(L-x,0),$$
$$\widetilde{u}(x,0) = -u(L-x,0),$$

to generate a left moving solitary wave, where $\eta(x,0)$ and $u(x,0)$ denote the functions in (5.2). The sum of the resulting two wave profiles gives the initial condition for the solitary wave collision test, as seen in Fig. 6a. Other parameters in the simulation are taken as follows: $\Delta x = 0.5$, $\Delta t = 0.1\Delta x$, and $L = 200$ for the length of the domain.

We apply the LDG method with alternating flux and SSPRK4 time discretization for the simulation. Figure 6 track the movement of the two peaks moving towards each other, combining to give a single peak, and then the waves moving past each other keeping the same profile as before the collision. Figure 6a shows the initial condition, where there are two peaks on the opposite ends of the domain. Figure 6b records the solution of $\eta(x,T)$ when the solitary waves traveled until time $T = 40$. We can observe that the amplitude and shape of the wave are kept well, and no oscillations are present. In Figure 6c, the waves have interacted at time $T = 60$, as the two main peaks are visible, with the depression in the

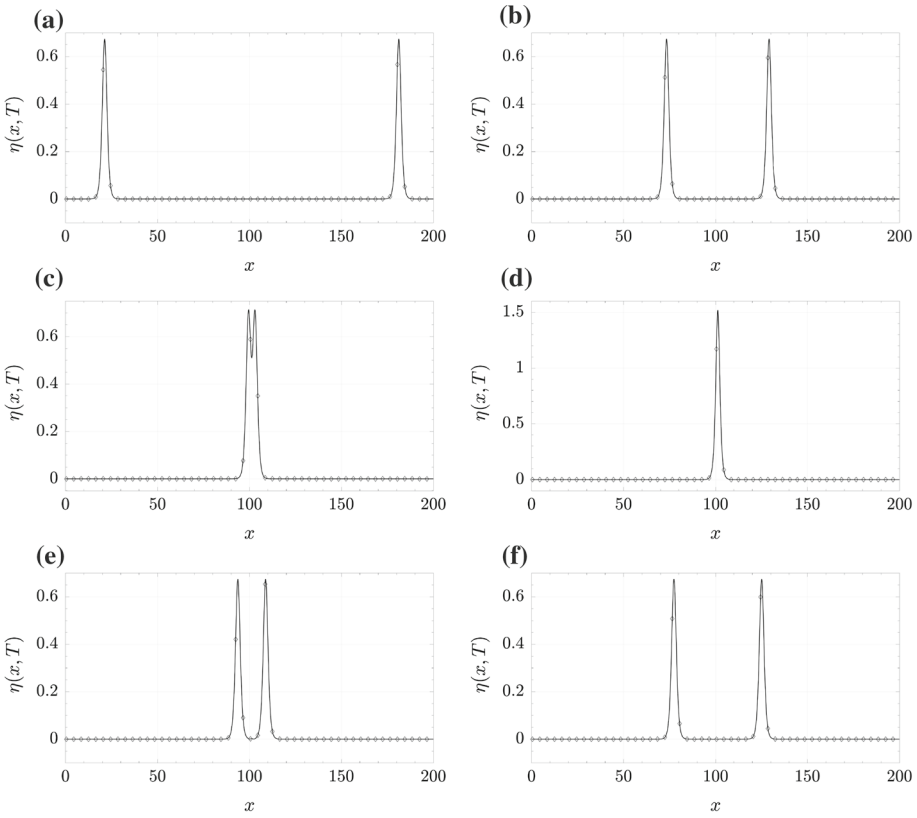

Fig. 6 Solitary wave collision for $\eta(x,t)$. **a** Waves at $T = 0$. **b** Waves at $T = 40$. **c** Waves at $T = 60$. **d** Waves at $T = 61.5$. **e** Waves at $T = 67.5$. **f** Waves at $T = 80$

center. At time $T = 61.5$, the two waves merge into one, as shown in Fig. 6d. In Fig. 6e, f, we can observe that after the interaction, it separates into two solitary waves moving away from each other, and with almost the same shape and amplitude as the waves before the collision.

6 Conclusion

In this paper, we have constructed LDG methods with both alternating flux and upwind flux for the coupled BBM system. This system has a Hamiltonian which is conserved for all time. We have shown that the LDG method with the alternating flux, coupled with the midpoint rule time discretization, provides a method which conserves the discrete Hamiltonian exactly, and the LDG method with the upwind flux dissipates the Hamiltonian. An optimal error estimate for the linearized system has been provided. Numerical examples are presented to illustrate the accuracy of the proposed methods in simulating the coupled BBM system. We hope that in future work, the choices of flux and methods presented here could be used to develop DG methods for a wider class of problems associated with the full abcd-Boussinesq system.

References

1. Alazman, A., Albert, J., Bona, J., Chen, M., Wu, J.: Comparisons between the BBM equation and a Boussinesq system. Adv. Differ. Equ. **11**(2), 121–166 (2006)
2. Bassi, F., Rebay, S.: A high-order accurate discontinuous finite element method for the numerical solution of the compressible Navier–Stokes equations. J. Comput. Phys. **131**, 267–279 (1997)
3. Benjamin, T., Bona, J., Mahony, J.: Model equations for long waves in nonlinear dispersive systems. Philos. Trans. R. Soc. Lond. A Math. Phys. Eng. Sci. **272**(1220), 47–78 (1972)
4. Bona, J., Chen, M.: A Boussinesq system for two-way propagation of nonlinear dispersive waves. Physica D **116**, 191–224 (1998)
5. Bona, J., Chen, M., Saut, J.: Boussinesq equations and other systems for small-amplitude long waves in nonlinear dispersive media. i. J. Nonlinear Sci. **12**, 283–318 (2002)
6. Bona, J., Chen, M., Saut, J.: Boussinesq equations and other systems for small-amplitude long waves in nonlinear dispersive media: II. The nonlinear theory. Nonlinearity **17**, 925–952 (2004)
7. Bona, J.L., Chen, H., Karakashian, O.A., Xing, Y.: Conservative discontinuous Galerkin methods for the Generalized Korteweg–de Vries equation. Math. Comput. **82**, 1401–1432 (2013)
8. Boussinesq, J.: Théorie de l'intumescence liquide appelée onde solitaire ou de translation se propageant dans un canal rectangulaire. Comptes Rendus de l'Acadmie de Sciences **72**, 755–759 (1871)
9. Chen, M.: Exact traveling-wave solutions to bidirectional wave equations. Int. J. Theor. Phys. **37**(5), 1547–1567 (1998)
10. Chen, R.M., Yue, L.: On the ill-posedness of a weakly dispersive one-dimensional Boussinesq system. J. d'Analyse Mathématique **121**(1), 299–316 (2013)
11. Chou, C.-S., Shu, C.-W., Xing, Y.: Optimal energy conserving local discontinuous Galerkin methods for second-order wave equation in heterogeneous media. J. Comput. Phys. **272**, 88–107 (2014)
12. Cockburn, B., Hou, S., Shu, C.-W.: The Runge-Kutta local projection discontinuous Galerkin finite element method for conservation laws IV: the multidimensional case. Math. Comput. **54**, 545–581 (1990)
13. Cockburn, B., Karniadakis, G., Shu, C.-W.: The development of discontinuous galerkin methods. In: Cockburn, B., Karniadakis, G., Shu, C.-W. (eds) Discontinuous Galerkin Methods: Theory, Computation and Applications, pp. 3–50. Lecture Notes in Computational Science and Engineering, Part I: Overview, vol. 11, Springer, Berlin (2000)
14. Cockburn, B., Lin, S.-Y., Shu, C.-W.: TVB Runge–Kutta local projection discontinuous Galerkin finite element method for conservation laws III: one dimensional systems. J. Comput. Phys. **84**, 90–113 (1989)
15. Cockburn, B., Shu, C.-W.: TVB Runge–Kutta local projection discontinuous Galerkin finite element method for conservation laws II: general framework. Math. Comput. **52**, 411–435 (1989)
16. Cockburn, B., Shu, C.W.: The local discontinuous Galerkin finite element method for convection-diffusion systems. SIAM J. Numer. Anal. **35**, 2440–2463 (1998)
17. Dougalis, V., Mitsotakis, D., Saut, J.: On initial-boundary value problems for a Boussinesq system of BBM–BBM type in a plane domain. Discret. Contin. Dyn. Syst. Ser. A **23**(4), 1191–1204 (2009)
18. Gottlieb, S.: On high order strong stability preserving Runge Kutta and multi step time discretizations. J. Sci. Comput. **25**(1 and 2), 105–128 (1999)
19. Liu, H., Huang, Y.-Q., Yi, N.-Y.: A direct discontinuous Galerkin method for the Degasperis–Procesi equation. Methods Appl. Anal. **21**, 83–106 (2014)
20. Liu, H., Xing, Y.: An invariant preserving discontinuous Galerkin method for the Camassa–Holm equation. SIAM J. Sci. Comput. **38**, A1919–A1934 (2016)
21. Reed, W.H., Hill, T.R.: Triangular mesh methods for the neutron transport equation. Technical Report LA-UR-73-479, Los Alamos Scientific Laboratory (1973)
22. Spiteri, R.J., Ruuth, S.J.: A new class of optimal high-order strong-stability-preserving time discretization methods. SIAM J. Numer. Anal. **40**, 469–491 (2002)
23. Wang, H., Shu, C.-W., Zhang, Q.: Stability and error estimates of local discontinuous Galerkin methods with implicit–explicit time-marching for advection–diffusion problems. SIAM J. Numer. Anal. **53**, 206–227 (2015)
24. Xing, Y., Chou, C.-S., Shu, C.-W.: Energy conserving local discontinuous Galerkin methods for wave propagation problems. Inverse Probl. Imaging **7**, 967–986 (2013)
25. Xu, Y., Shu, C.-W.: Error estimates of the semi-discrete local discontinuous galerkin method for nonlinear convection–diffusion and KdV equations. Comput. Methods Appl. Mech. Eng. **196**, 3805–3822 (2007)
26. Xu, Y., Shu, C.-W.: Local discontinuous Galerkin methods for high-order time-dependent partial differential equations. Commun. Comput. Phys. **7**, 1–46 (2010)